Dual targeting of MAPK and PI3K pathways unlocks re-differentiation of Braf-mutated thyroid cancer organoids

Hélène Lasolle [1], Andrea Schiavo [1], Adrien Tourneur[1], Pierre Gillotay [1], Bárbara de Faria da Fonseca [1], Lucieli Ceolin [1, 6], Olivier Monestier [1], Benilda Aganahi [1], Laura Chomette [1], Marina Malta Letro Kizys [1], Lieven Haenebalcke [2], Tim Pieters [2, 3], Steven Goossens [2, 4], Jody Haigh [2, 5], Vincent Detours [1], Ana Luiza Silva Maia [6], Sabine Costagliola [1] and Mírian Romitti [1*]

[1] Institut de Recherche Interdisciplinaire en Biologie Humaine et Moléculaire (IRIBHM), Université Libre de Bruxelles (ULB), Brussels, Belgium

[2] VIB, Flanders Institute for Biotechnology, Ghent University, Ghent, Belgium

[3] Department of Biomolecular Medicine, Faculty of Medicine and Health Sciences, Ghent University, Ghent, Belgium

[4] Department of Diagnostic Sciences, Faculty of Medicine and Health Sciences, Ghent University, Ghent, Belgium

[5] CancerCare Manitoba Research Institute, Department of Pharmacology and Therapeutics, Rady Faculty of Health Sciences, University of Manitoba, Winnipeg, Manitoba, Canada

[6] Thyroid Section, Endocrine Division, Hospital de Clínicas de Porto Alegre (HCPA), Universidade Federal do Rio Grande do Sul (UFRGS), Porto Alegre, Brazil

* Corresponding author: mirian.romitti@ulb.be

The authors declare no potential conflicts of interest

Thyroid cancer is the most common endocrine malignancy and several genetic events have been described to promote the development of thyroid carcinogenesis. Besides the effects of specific mutations on thyroid cancer development, the molecular mechanisms controlling tumorigenesis, tumor behavior, and drug resistance are still largely unknown. Cancer organoids have been proposed as a powerful tool to study aspects related to tumor development and progression and appear promising to test individual responses to therapies. Here, using mESC-derived thyroid organoids, we developed a $Braf^{V637E}$-inducible model able to recapitulate the features of papillary thyroid cancer in vitro. Overexpression of $Braf^{V637E}$ rapidly leads to MAPK activation, cell dedifferentiation, and disruption of follicular organization. $Braf^{V637E}$-expressing organoids show a transcriptomic signature for p53, focal adhesion, ECM-receptor interactions, EMT, and inflammatory signaling pathways. Finally, PTC-like thyroid organoids were used for drug screening assays. The combination of MAPK and PI3K inhibitors reversed *Braf* oncogene-promoted cell dedifferentiation while restoring thyroid follicle organization and function *in vitro*. Our results demonstrate that pluripotent stem cells-derived thyroid cancer organoids can mimic tumor development and features while providing an efficient tool for testing novel targeted therapies.

INTRODUCTION

Pluripotent Stem Cells (PSCs) emerged as a model to dissect and recapitulate the molecular events and gene networks that regulate cell fate determination, cell differentiation and organogenesis. Guided differentiation of PSCs into 3D organized tissue by inducible overexpression of specific transcription or growth factors and inhibitors allows the derivation of *in vitro* organoids and the understanding of mechanisms regulating cell differentiation and tissue formation[1]. Due to their remarkable

51 self-organizing structures and functional properties, organoids technology became a
52 powerful tool to model organ development and disease 'in a dish' [2,3].

53 In the last decade, the use of organoids for cancer research emerged and opened
54 new possibilities to better understand tumor behavior. Initially, colon, prostate,
55 pancreatic, ovarian, lung and thyroid cancer-derived organoids have been efficiently
56 generated, which resemble phenotypically and genetically the tumor of origin[4–13].
57 Currently, a large set of healthy and tumour matching organoids has been generated and
58 is available through biobanks. These patient-derived organoids are particularly interesting
59 in testing individual responses to therapies[8,13,14].

60 Recently, studies have reported the generation of cancer models arising from
61 healthy (adult stem cells or aSCs and PSCs) organoids by controlling oncogene
62 expression[15–17]. By using gene expression manipulation tools, such as shRNA and
63 CRISPR-Cas9, murine stomach cancer ($Cdh1^{-/-}$; $Tp53^{-/-}$)[18], murine and human colon
64 cancer (APC, TP53, KRAS and Smad4 mutations)[15,16,19], human pancreatic cancer
65 (KRAS and/or TP53 mutations)[4,20] and human lung adenocarcinoma organoids (HER2
66 overexpression) could be efficiently generated[17]. Compared to patient-derived organoids,
67 healthy stem cells-derived cancer organoids are suitable to address additional questions
68 such as precise effects of oncogenes and early events driving tumorigenesis; the role of
69 cancer stem cells on tumor induction, genomic stability, the effect of treatments at
70 different stages of carcinogenesis and screening for new therapeutical tools[21]. Besides,
71 they allow multiple reproducible experiments free from inter-individual variability.

72 Thyroid cancer is the most frequent endocrine malignancy, and several genetic
73 events have been described as driving thyroid carcinogenesis. Papillary thyroid
74 carcinoma (PTC) is the most common malignant thyroid tumor[22], and aberrant activation
75 of the MAPK pathway is a hallmark[23]. The $BRAF^{V600E}$ mutation is the most frequent

genetic event, accounting for around 50% of PTCs[24–26] and results is an oncogenic protein with markedly elevated kinase activity that constitutively induces MEK/ERK signaling transduction[27–29].

BRAF-mutated thyroid tumors are often less differentiated, mainly due to the lower expression levels of thyroid functional genes *NIS, TSHR, TG* or *TPO,* leading to a low Thyroid Differentiation Score (TDS)[30]. This dedifferentiated state is associated with a worse clinical condition and with a higher rate of radioactive iodine (RAI) refractory tumors[31,32]. However, its impact on prognosis is still uncertain, as $BRAF^{V600E}$ alone has not been proven to be an independent prognostic factor[33,34]. On the other hand, *BRAF* and *TERT* promoter mutated tumors have been associated with higher specific mortality[35]. Also, studies have shown a small proportion (around 20%) of $BRAF^{V600E}$ mutated tumors presenting a higher level of differentiation associated with a less aggressive behavior and a preserved RAI uptake ability[30,36]. This suggests a possible cell heterogeneity among the $BRAF^{V600E}$ mutated tumors.

Some years ago, our group showed the generation of functional 3D thyroid tissue derived from mouse embryonic stem cells (mESC)[37] and, recently human thyroid organoids were generated using the same approach[38]. The differentiation protocol relies on transient induction of *Nkx2.1* and *Pax8* thyroid transcription factors allowing an efficient generation of thyroid follicular cells organized into three-dimensional follicular structures capable of thyroid hormone production *in vitro* and *in vivo*. This model and further developed thyroid organoids from healthy mouse and human PSCs/aSC[39–49] open new perspectives to explore thyroid development processes and to model thyroid diseases, including thyroid cancer.

So far, efficient, fast and cost-effective tools are lacking to functionally characterize a large set of candidate genes in the context of thyroid carcinogenesis.

101 Thyroid cancer organoids/spheroids models have been recently described based on
102 patient tumor-derived models[50–54]. Patient-derived organoid might be used to study
103 patient-specific tumor behavior and the treatment response on a case-to-case basis. It is
104 patient-to-patient dependent with high heterogeneity and low reproducibility. It is limited
105 by the accessibility to samples and since it is derived from an already established tumor,
106 it is not suitable to study mechanisms related to cancer development and drug resistance
107 acquisition. Saito et al. described a mouse model of poorly differentiated thyroid
108 carcinoma obtained after transplantation of thyroid organoids derived from Tp53
109 knockout mice with NRAS activating mutation overexpression[12]. Recently, Veschi *et al.*
110 [55] generated of PTC and FTC organoids models by inducing *BRAF*, *NRAS* and *TP53*
111 mutations in thyroid progenitors derived from hESC. After transplantation, the tumors
112 generated resemble Papillary and Follicular tumors and, transcriptomics analysis
113 suggested a role of Kisspeptin receptor (KISS1R) in cooperation with Tissue Inhibitor of
114 Metalloproteinase 1 (TIMP1)/Matrix metallopeptidase 9 (MMP9)/Cluster of
115 differentiation 44 (CD44), on tumor development and progression[55].

116 Here, we aim to develop an *in vitro* PTC organoid model to screen for targets and
117 drugs by taking advantage of our model of thyroid generation by inducible expression of
118 $Braf^{V637E}$ mutation in mouse ESC-derived functional thyroid follicles.

119

120 **RESULTS**

121 **mESC_$BRAF^{V637E}$ cell line generation and characterization**

122 We combined the previously described mESC transient induction thyroid differentiation
123 strategy (Antonica, 2012) with a $Braf^{V637E}$-ERT^2 inducible model (Ortiz, 2013) to
124 generate a double-inducible recombinant mESC_$BRAF^{V637E}$ cell line. The resulting
125 mESC_Nkx2-1/Pax8_bTg_$Braf^{V637E}$_ERT^2 clones were initially selected and

126 characterized by the response to doxycycline (Dox) treatment, confirmed by the
127 overexpression of Nkx2-1 and Pax8; and ability to spontaneously differentiate into cells
128 from the three germ-layers (Supplementary Fig. 1A-C). In addition, a control mESC line
129 was generated in which Braf^{V637E}_ERT^{2} system was replaced by the eGFP sequence.
130 Similarly, the control line responded properly to Dox induction and maintained the
131 pluripotency capacity (Supplementary Fig. 1D-F).
132
133 **Thyroid differentiation protocol**
134 The capability of the new cell line to generate thyroid follicles and express the Braf^{V637E}
135 oncogene was demonstrated following the mESC thyroid differentiation protocol[37,56,57].
136 Since we used a newly modified mESC line, the steps of the differentiation protocol were
137 tested and adapted accordingly (Fig. 1A). Here, using the mESC_Nkx2-
138 1/Pax8_bTg_Braf^{V637E} line, we observed that Dox stimulation for 5 days leads to higher
139 exogenous and endogenous *Nkx2-1*, *Pax8* and *Tg* mRNA (day 9; Supplementary Fig. 2E)
140 compared to 3 or 4 days of treatment (Supplementary Fig. 2A-D). Similar results were
141 obtained using the control mESC line (data not shown). Next, two weeks of treatment
142 with cAMP (from day 9 to 23) markedly induced the expression levels of *Nkx2-1, Pax8,*
143 *Tg, TshR, Nis* and *Tpo* when compared to the control (-Dox -cAMP) (Fig. 1B).
144 Accordingly, immunofluorescence staining showed follicular organized Nkx2-1 and Tg-
145 expressing cells (Fig. 1C), in which the functionality is demonstrated by intraluminal
146 iodinate-Tg (Tg-I) accumulation (Fig. 1D). Since our protocol also generates other cell
147 types than thyroid[57], a follicle enrichment step was added to the protocol to enrich the
148 follicular structures and induce Braf-oncogene in a purer population. This protocol led to
149 an increase of thyroid markers levels (Fig. 1E) when compared to the non-enriched
150 control condition, while the follicular structure and functionality were preserved as

151 demonstrated by Nkx2-1, Nis and Tg-I staining (Fig. 1F-G). Notably, after re-embedding
152 in Matrigel (MTG), follicles could be maintained in culture for at least 28 additional days
153 without major histological changes (data not shown).
154
155 **Braf^{V637E} induction on thyroid organoids leads to PTC-like phenotype**
156 To ensure that Braf^{V637E} oncogene is expressed specifically among follicular thyroid cells,
157 we used the bovine Tg (bTg) as a promoter controlling Braf^{V637E}_ERT^{2} expression.
158 Effectively, exogenous *Braf^{V637E}* mRNA expression was rapidly induced after Dox
159 treatment (Day 9; Supplementary Fig. 2E), maintaining the expression levels stable over
160 time (Fig.1B and Supplementary Fig. 3A), while *Tg* mRNA expression increased
161 following the differentiation program (Supplementary Fig. 3A). Even if *Braf^{V637E}*
162 expression is driven by the bTg promoter, the Braf-mutated protein is not
163 active/phosphorylated since it is maintained in the nucleus in an inactive complex with
164 HSP90. The addition of 4OHT induces nuclear translocation of the Braf mutant to the
165 cytoplasm (NES signal), then driving MAPK activation[58] (Fig. 2A). Indeed, 24 hours
166 after 4OHT addition, we observed an increase in ERK phosphorylation (pERK) compared
167 to the control condition (cAMP), which was maintained after 7 days of continuous 4OHT
168 treatment (Fig. 2B). To assess Braf-induced cell proliferation, flow cytometry analysis
169 performed after 6 days of 4OHT treatment demonstrated an increased proportion of
170 Nkx2-1/BrdU+ cells among the Braf^{V637E}-expressing condition (4OHT) compared to the
171 control (cAMP) (Fig. 2C).
172 One of the hallmarks of thyroid cancer development is the downregulation of
173 thyroid differentiation markers[28,59]. Indeed, the activation of Braf^{V637E} rapidly led to a
174 progressive time-dependent decrease of *Tpo*, *TSHR* and *Tg* mRNA expression (Fig. 2D-
175 F and Supplementary Fig. 3B), detected as early as 6 hours after 4OHT addition (Fig.

176 2D). Notably, more significant downregulation was observed after 48 hours and
177 maintained for at least 7 days (Fig. 2E-F, respectively). As described among PTCs, in our
178 model, the expression of thyroid transcription factors *Pax8* and *Nkx2-1* was also globally
179 maintained. Conversely, *Lgals3 (Galectin 3)* expression, which has been suggested as a
180 marker for thyroid malignancies and, more specifically, for PTC[60], was significantly
181 increased in both time points (Fig. 2E-F). Also, an increase in Fibronectin 1 (*Fn1*)
182 expression, associated with aggressive thyroid cancer[61,62], was observed after 7 days of
183 $Braf^{V637E}$ induction, suggesting a more advanced dedifferentiated cell state in our
184 organoid model (Fig. 2F). Similar results were obtained when cells were differentiated
185 using hrTSH instead of cAMP, and $Braf^{V637E}$ was induced in such conditioned media,
186 indicating that the phenotype is not dependent of TSH signaling (data not shown).

187 Histological analysis performed after 48 hours of continuous activation of
188 $Braf^{V637E}$ by 4OHT demonstrated disruption of the follicular organization in non-enriched
189 thyroid organoids compared to the control condition (cAMP) (Fig. 3A). Nkx2-1 and Tg
190 staining revealed that $Braf^{V637E}$ oncogene strongly disturbs thyroid follicles forming
191 elongated and unorganized structures. In addition, heterogeneous expression of Tg was
192 observed among the Nkx2-1 cells. Further analysis, performed in follicle enriched
193 population, confirmed the effect of *Braf* oncogene in promoting cell dedifferentiation and
194 loss of follicle organization. Tg levels were overall reduced and heterogeneous among
195 the unorganized Nkx2-1+ cells (Fig. 3B). Interestingly, the cell disorganization caused
196 by Braf oncogene might pass by an initial expansion of the follicular size with infiltration
197 of Nkx2-1 cells inside of the lumen compartment, which also presents a heterogeneous
198 distribution of Tg (Supplementary Fig. 3C), since this feature was observed among some
199 "follicular-like" remaining structures after 48 h of 4OHT treatment. Reassuringly,
200 staining for E-Cadherin (epithelial) and Zo-1 (intra-luminal) adhesion markers showed

201 that Braf^{V637E}-expressing cells (Nkx2-1) are not able to preserve polarization and,
202 consequently lumen space is not well defined in most of the structures (Fig. 3C, D,
203 respectively). Therefore, the functionality of those cells was impaired and, Tg-I
204 accumulation was significantly reduced compared to the control condition (Fig. 3E). Of
205 note, despite the strong effect of Braf^{V637E} oncogene on thyroid follicles disruption, we
206 observed that few follicles still preserved a certain degree of organization (Supplementary
207 Fig. 3D) after 48 h of 4OHT treatment. As expected, after 7 days of Braf^{V637E} continuous
208 stimulation, a higher level of cell dedifferentiation and lack of organization could be
209 detected, with a lower proportion of the Nkx2-1 cells expressing Tg compared to control
210 (Fig. 3F) and to the previous time point (48 h; Fig. 3A). The above-described experiments
211 were also performed using the control TRE-Nkx2-1-Pax8_bTg-eGFP cell line. Adding
212 4OHT to mature follicles (from day 27 to day 36) did not impair the levels of the thyroid
213 differentiation markers and the follicles organization (Supplementary Fig. 3E, F). On the
214 other hand, slight induction of *Nkx2.1, Pax8, Tg, TshR, Tpo and Nis* levels was observed
215 under cAMP co-treatment with 4OHT (Supplementary Fig. 3E).
216
217 **Effect of transient Braf^{V637E}-induction on cell differentiation**
218 Since our system for Braf^{V637E} activation is dependent on continuous treatment with
219 4OHT, we transiently treated the cells with 4OHT for 2 days, followed by 5 days of
220 culture in a 4OHT-free medium (cAMP) in order to explore if the oncogenic effect is
221 maintained when the protein is not active. Surprisingly, we did not observe the recovery
222 of *Nkx2-1, TSHR, Tg* or *Tpo* gene expression levels (Fig. 4A-E) after 4OHT removal.
223 However, *Pax8* and *Slc5a5/Nis* expression was partially recovered (Fig. 4F), confirming
224 the specific inhibitory effect of *Braf* oncogene on *Slc5a5/Nis* expression. These findings

225 indicate that *Nis* regulation mechanisms are maintained in our system and suggest it as a
226 tool for Nis-reactivation studies.
227
228 **Screening for Nis re-expression using signaling pathways inhibitors**
229 Studies in mouse models and humans have demonstrated that tumors carrying *Braf*
230 mutations show reduced expression of *Nis* and, consequently a higher rate of radioiodine
231 (RAI) refractoriness[28,31,63]. Here, taking advantage of our PTC organoid model, we aim
232 to explore new strategies to reactivate *Nis* expression in Braf^{V637E}-expressing cells by
233 screening distinct categories of inhibitors previously described to be involved in *Nis*
234 regulation [64,65]. PD0325901 (MEK inhibitor), LY204002 (PI3K inhibitor), VPA (HDAC
235 inhibitor), NAC (N-acetyl cysteine, antioxidant compound), 5-AZA-2' deoxycytidine and
236 RG108 (DMNT inhibitors) were tested isolated and/or in combination for 3 days (in
237 addition to cAMP+4OHT) using Braf^{V637E}-expressing organoids (after 4 days of
238 cAMP+4OHT treatment; Fig. 5A). Initially, we observed that VPA alone was the only
239 treatment able to completely restore *Nis* expression levels (Fig. 5B, C and Supplementary
240 Fig. 4A). However, when combined, PD0325901 and LY204002 inhibitors; PD0325901,
241 LY204002 and VPA; and PD0325901 and Nac resulted in a great increase of *Nis* mRNA
242 (Fig. 5B, C and Supplementary Fig. 4A). IF staining shows Nis protein re-expression
243 among Braf^{V637E}-induced cells treated with VPA alone, but localization was not restricted
244 to the membrane. In contrast, when cells were treated with MEK of PI3K inhibitors,
245 associated or not with VPA, we observed Nis protein at the apical membrane and
246 surprisingly, restored the follicular structure (Fig. 5C).
247
248 **MAPK and PI3K signaling inhibition cause Braf-induced cells redifferentiation and**
249 **function recovery**

250 Since we observed that HDAC, MEK and PI3K inhibition seems to favor follicle
251 reorganization, we evaluated if such treatments also induce cell redifferentiation and
252 function recovery. Initially, we analyzed the gene expression levels of thyroid
253 differentiation markers strongly affected by Braf-induction. The effects of isolated and
254 combined drugs on *Tg, TSHR, Tpo, Nkx2-1* and *Duox* genes appear variable and pathway-
255 dependent (Supplementary Fig. 4B-F). As with *Slc5a5/Nis*, MEK and PI3K inhibition in
256 combination with or without VPA resulted in complete recovery of *Tg*, *TSHR* and *Tpo*
257 mRNA levels (Fig. 6A-C), indicating cell redifferentiation. While *TSHR* levels can be
258 restored by treatment with isolated inhibitors (Fig. 6B), *Tpo* expression appears to be
259 dependent on PI3K signaling (Fig. 6C). On the other hand, *Tg* mRNA expression is
260 recovered just when the inhibitors are used in combination (Fig. 6A). Indeed,
261 immunostaining showed that isolated inhibitors could not restore Tg levels. Nevertheless,
262 a higher proportion of Tg-expressing cells was observed with the MEK inhibitor
263 PD0325901 (Supplementary Fig. 4G). Conversely, combined MEK and PI3K inhibitors
264 restored Tg protein levels and generated a similar proportion of expressing follicles as
265 under the cAMP condition (Fig. 6D-E).
266 Considering that inhibition of MEK and PI3K pathways (+/-VPA) promote recovery of
267 thyroid redifferentiation and follicular organization, we tested the functionality of
268 reorganized follicles. Remarkably, we observed an accumulation of Tg-I in the lumen of
269 follicles treated with the combinations of inhibitors (Fig. 6F). The organification assay
270 confirmed that the co-treatment restored iodide uptake and ^{125}I binding to proteins
271 resulting in organification levels comparable to the control (Fig. 6G-I).
272

273 **Transcriptomic characterization of the PTC model and drug screening**

274 Transcriptomic analysis of cAMP, cAMP+4OHT and cAMP+4OHT+PD+LY (Fig. 5A)

275 confirmed downregulation of thyroid genes under Braf-oncogene stimulation (4OHT
276 condition) whereas, global recovery of expression was observed under inhibitors
277 treatment (Fig. 7A). Accordingly, thyroid differentiation scores (TDS and enhanced
278 (e)TDS) were decreased under $Braf^{V637E}$ induction while they recovered in the presence
279 of inhibitors (Fig. 7B). Conversely, the ERK activation score was higher in the $Braf^{V637E}$
280 samples and decreased sharply under inhibitor conditions (Fig. 7C). Since bulk RNAseq
281 was performed using the follicle-enriched population, the presence of non-thyroid cells
282 is reduced compared with the whole original organoids but still present. It may explain
283 the modest increase in ERK score among Braf-activated cells while the apparent decrease
284 under the condition with inhibitors reflects the effect of the treatment on each cell type.
285 Differential expression analysis identified 321 Differential Expressed Genes (DEGs; 156
286 upregulated and 165 downregulated genes) in the 4OHT condition compared to cAMP;
287 and 853 DEGs in inhibitors compared to 4OHT (287 upregulated and 566 downregulated
288 genes). Gene enrichment classification analysis of DEGs results is presented in Fig. 7D-
289 G. Briefly, among the upregulated genes in Braf-induced compared to control, we
290 observed gene signature for the hyperactivation of PI3K-AKT-mTOR, TNF, and
291 cytokines signaling and promotion of Epithelial-Mesenchymal transition (EMT) (Fig.
292 7D). While genes associated with thyroid hormone production, TGF-beta, Wnt/Beta-
293 Catenin pathway, and regulation of angiogenesis were down-regulated (Fig. 7E).
294 Conversely, the inhibitor's treatment, compared to 4OHT condition, evidenced
295 upregulation of genes associated with thyroid hormone production, cell-cell contact,
296 extra-cellular matrix organization, and angiogenesis processes (Fig. 7F), while PI3K,
297 MAPK, TNF, cytokines signaling, ECM-receptor interactions and EMT-related genes
298 were downregulated (Fig. 7G).
299

300 **DISCUSSION**

301 Here, we described a Braf-oncogene derived thyroid cancer organoid model
302 recapitulating patient tumor features. *In vitro* thyroid cancer models that recapitulate
303 tumor development and behavior can facilitate the identification of early tumor drivers
304 and enable the screening of several new drugs for the treatment of thyroid cancer without
305 the need to use too many animal models. Combining our previous thyroid organoid model
306 derived from mESCs with an inducible system, the $Braf^{V637E}$ oncogene could be induced
307 explicitly in mature Tg-expressing cells to obtain a 3D *in vitro* cancer model.
308 Overexpression of $Braf^{V637E}$ rapidly led to MAPK activation with increased pERK, cell
309 dedifferentiation and disruption of follicular organization. Similar effects have been
310 described in genetically modified mouse models[28,59,66]. Furthermore, the gene expression
311 signature of our cancer organoids confirmed the findings found in the PTC samples,
312 which also showed enrichment of genes associated to p53, focal adhesion, ECM-receptor
313 interactions, EMT and inflammatory pathways[67–69].

314 Activating mutations in the *BRAF* gene are found in approximately 7% of all solid
315 human tumors, particularly common in PTCs, ATCs and melanomas. In addition, they
316 have been reported less frequently in colorectal cancers (CRCs), lung cancers, pediatric
317 low-grade gliomas (PLGGs), glioblastomas, breast cancers and serous ovarian cancers[70–
318 76]. In PTCs and melanomas, $BRAF^{V600E}$ mutation seems to be associated with a higher
319 degree of dedifferentiation and more aggressive histological patterns. However, its
320 prognostic role is still debated as it was not found independently of histological
321 features[33,34]. Nevertheless, studies suggest that $BRAF^{V600E}$ might predict response to
322 tyrosine kinase inhibitors (TKIs) in melanoma and lung cancer[77,78].

323 Surgery remains the first choice for thyroid cancer therapy. Recommended post-
324 operative treatment includes TSH suppression and RAI ablation, particularly as adjuvant

325 treatment for patients at high risk for tumor recurrence and to treat patients with
326 persistent/recurrent or metastatic disease[79]. The benefit of RAI has been demonstrated in
327 patients by reducing the risk of recurrence and disease-related mortality[80]. However,
328 approximately two-thirds of metastatic DTC become radioiodine refractory (RR-DTC),
329 defined by the absence of iodine uptake or tumor progression despite uptake[81,82]. There
330 is no curative treatment for radioiodine refractory DTCs. The recommended first-line
331 systemic treatment when local therapies are not possible is targeted therapies using
332 mainly multitarget TKIs, such as Lenvatinib showed a progression-free survival of 18
333 months [63,83–85]. However, it leads to frequent resistance and adverse effects.

334 NIS, a basal membrane iodide transporter, plays a critical role in radioiodine
335 accumulation in DTC cells and its level is closely related to response to RAI (I^{131}) therapy.
336 Studies in mouse models and humans have shown that the presence of *BRAF* mutations
337 results in lower *Nis* levels and, consequently a higher rate of RAI-refractory tumours[28,31].
338 Here, we confirmed that this regulation is preserved in our cancer organoids, as disruption
339 of *Braf* activation led to in recovery of *Nis* levels. As TKIs, retinoic acids (RA), histone
340 deacetylase inhibitors (HDAC), peroxisome proliferator-activated receptor-gamma
341 (PPARG) have been tested to promote redifferentiation and *NIS* re-expression of RR-
342 DTCs, to suggest RAI treatment after a short, targeted treatment[83,86–88]. This strategy
343 could lead to tumor response while limiting adverse effects and, several clinical trials are
344 ongoing. However, the re-expression of NIS is insufficient to explain the response to
345 redifferentiation therapeutics and RAI treatment. Membrane trafficking and the cellular
346 machinery that concentrate and retain iodine must be preserved[89] in a follicular
347 organization. Our model is proving to be a potential tool for redifferentiation studies
348 because of its ability to test large sets and combinations of treatments and to assess
349 follicular reorganization and iodide organification capacity using a functional assay that

350 is likely to be more strongly associated with response to RAI treatment than *NIS* mRNA
351 levels. Braf^{V637E}-expressing cells treated with VPA, MAPK and PI3K inhibitors showed
352 re-expression of *Nis* and corresponding uptake of radioactive iodide. Interestingly, the
353 combination of inhibitors also promoted the restoration of thyroid markers, follicular
354 organization, and iodide organification ability. Interestingly, an ongoing clinical trial tests
355 the effect of BKM120, a PI3K inhibitor, in patients with progressive, metastatic,
356 refractory, follicular or poorly differentiated thyroid cancers (NCT01830504). However,
357 the association with MAPK inhibitors is still not evaluated in patients with thyroid cancer.
358 In *BRAF*-mutated tumors, studies have shown that the combination of TKIs
359 therapies appears more effective and circumvents primary and acquired resistance to TKI
360 therapy. Often, resistance is due to reactivation of the MAPK/ERK pathway or activation
361 of other signaling pathways such as PTEN, NF-1 or RAS. It may also result from the
362 hyperactivation of tyrosine kinase receptors, such as PDFRβ, IGF-1R and HGF, which
363 lead to activation of the AKT/PI3K pathway[90]. Studies in patients with advanced
364 melanoma carrying a BRAF^{V600E} mutation have shown that combining BRAF and MEK
365 inhibitors resulted in a higher rate of complete/partial responses and median progression-
366 free survival compared with monotherapy groups[91–93]. Such significant results lead to the
367 use of drug combinations as standard treatment for the patients[94,95].
368 In summary, we have developed a Braf oncogene-expressing thyroid cancer in
369 vitro organoid model from mESCs that recapitulates transcriptomic and histological
370 features of PTCs at early and advanced stages. Moreover, we demonstrated that the
371 combination of MEK and PI3K inhibitors promotes *Nis* re-expression and cell re-
372 differentiation leading to the restoration of follicular structures and thyroid functionality.
373 Considering the robustness of this *in vitro* model, which allows controlled induction of
374 the major thyroid oncogene in a three-dimensional system, its efficiency and simplicity,

375 our model can be used to study mechanisms associated with thyroid cancer development
376 and progression, thyroid redifferentiation, and drug screening.
377
378 **MATERIAL AND METHODS**
379
380 **Cell culture and mESC_Braf^{V637E} line generation**

381 The previously genetically modified G4 RosaLuc mouse embryonic stem cell line
382 (mESC)[96] was initially cultured on gamma-irradiated mouse embryonic fibroblasts
383 (MEFs) feeder using mouse stem cell medium[37,57] and incubated at 37 °C, 5 % CO^2 and
384 >95 % humidity. To insert the target sequences into the modified Rosa26 locus of G4
385 RosaLuc mESCs, around $1x10^5$ cells were transfected using the Flpe expressing vector[96]
386 and the target vector containing the rtTA-TRE induction system, thyroid transcription
387 factors, Nkx2-1 and Pax8 and bTg-NES-Braf^{V637E}-ERT^2 sequences (Supplementary Fig.
388 1A) following the lipofectamine 3000 protocol (Thermo Scientific). The Braf^{V637E}
389 mutation here used for mouse cells is equivalent to the human BRAF^{V600E} mutation[58].
390 G418 (300 µg/ml) was applied 48 h after transfection, typically for 10 days, and
391 individual clones were picked and further expanded. Clones were screened for by
392 immunofluorescence for Nkx2-1 and Pax8 expression induction after three days of
393 incubation with 1 µg/ml Doxycyclin (Dox) (Supplementary Fig. 1B). Positive clones
394 were then characterized according to pluripotency maintenance (Supplementary Fig. 1C),
395 *Nkx2-1* and *Pax8* expression, and efficiency of thyroid differentiation. In addition, we
396 generated an mESC control line where the sequences of NES-BRAF^{V637E}-ERT^2 were
397 replaced by the eGFP sequence, resulting in the TRE-Nkx2-1-Pax8_bTg-eGFP line
398 (Supplementary Fig. 1D). The mESC control line generation, selection and
399 characterization were performed as described above (Supplementary Fig. 1E, F).

400 **Thyroid differentiation protocol**

401 G4 RosaLuc TRE-Nkx2-1-Pax8_bTg-NES-Braf^{V637E}-ERT^{2} and TRE-Nkx2-1-
402 Pax8_bTg-eGFP cells were cultured and differentiated as described previously by
403 Antonica *et al.* (2012)[37] with few modifications. Briefly, embryoid bodies (EBs),
404 generated by hanging drops were collected after four days and embedded in growth factor
405 reduced Matrigel (GFR MTG; BD Biosciences); 50µl MTG drops (containing around 20
406 EBs) were plated into 12-wells plates. EBs were differentiated using a differentiation
407 medium initially supplemented with 1µg/ml of Doxycycline (Sigma) for five days,
408 followed by two weeks of maturation induction by using 0.3 µmol of 8-Br-cAMP
409 (BioLog Life Science Institute) or 1mU ml^{-1} of thyrotropin (hrTSH; Genzyme). Thyroid
410 differentiation and functionality were evaluated by transcriptomics (RT-PCR and bulk
411 RNA sequencing), immunofluorescence, and iodide organification.

412

413 **Braf^{V637E} induction and drug screening**

414 After full thyroid maturation (Day 25), MTG drops were washed twice with Hanks's
415 balanced salt solution (HBSS, containing calcium and magnesium; Invitrogen) and
416 incubated in an HBSS solution (1 ml per well) containing 10 U/ml of dispase II (Roche)
417 and 125 U/ml of collagenase type IV (Sigma) for 30 min at 37°C. Then the enzymes were
418 inactivated by adding 10% FBS and cells were centrifuged at 500g for 3 min. Cells were
419 rinsed twice with HBSS, and the follicles population was enriched by filtering using 30
420 µm (single cell removal) and 100 µm reverse strainer (Pluriselect). Finally, enriched
421 structures were re-embedded in GFR MTG (50µl) and plated into 12-well plates. Twenty-
422 four hours later, cells were incubated with 1 µM of 4-Hydroxytamoxifen (4OHT) (Sigma)
423 and 8-Br-cAMP or hrTSH for 24h, 48h or 7 days to promote Braf^{V637E}-induced
424 phosphorylation of MAPK pathway[58].

425 In addition, Braf-induced thyroid organoids (previously treated for four days with 4OHT)
426 were cultured with distinct compounds, previously suggested to regulate Nis re-
427 expression and inhibit *Braf* oncogenic effects[64,65]. Among the screened drugs, several
428 cell processes were targeted by the following compounds: PD0325901 (MEK inhibitor;
429 250nM; Stem Cell), LY204002 (PI3K inhibitor; 5µM; Selleckchem), VPA (HDAC
430 inhibitor; 250µM; Sigma), NAC (N-acetyl cysteine, antioxidant compound; 2mM;
431 Sigma), 5-AZA-2' deoxycytidine (DNA methyltransferase (DMNT) inhibitor; 1µM;
432 Sigma) and RG108 (DMNT inhibitor; 10µM; Sigma).
433
434 **Flow cytometry - Proliferation assay**
435 Control condition (4OHT-) and organoids treated with 4OHT for 6 days were treated with
436 BrdU (1mM) for 3 hours, collected and prepared for immunostaining as follows: Matrigel
437 drops (at least five samples per condition) were first digested with HBSS solution
438 containing 10 U/ml dispase II and 125 U/ml collagenase type IV for 30-60 min at 37°C;
439 then a single cell suspension was obtained by dissociation with TripLE Express for 10-
440 15 min incubation at 37°C, the enzymes were inactivated by addition of differentiation
441 medium. After centrifugation, samples were rinsed with PBS, and then the BrdU Flow
442 Kit staining protocol (BD) was used according to the manufacturer's instructions. In order
443 to identify the BrdU incorporated cells among the thyroid population, cells were also
444 stained using primary Nkx2-1 antibody (1:100; Abcam; RRID:AB_1310784) and anti-
445 rabbit IgG Alexa fluor 647-conjugated secondary antibody (1:300; Jackson
446 Immunoresearch; RRID:AB_2492288). Non-stained and only secondary-incubated cells
447 were used as a negative control for gate strategy. LSR-Fortessa X-20 flow cytometer was
448 used for quantification, and BD FACSDiva software (RRID:SCR_001456) was used for
449 the analysis. Data are presented as a percentage of positive cells.

450 **Immunofluorescence staining**

451 Organoids embedded in MTG were fixed in 4% paraformaldehyde (PFA; Sigma) for 1 h
452 at room temperature (RT) and washed three times in PBS. Blocking was performed using
453 a solution of PBS containing 3% bovine serum albumin (BSA; Sigma), 5% horse serum
454 (Invitrogen) and 0.3% Triton X-100 (Sigma) for 30 min at RT. The primary and
455 secondary antibodies were diluted in a solution of PBS containing 3% BSA, 1% horse
456 serum and 0.1% Triton X-100. Primary antibodies were incubated overnight at 4°C
457 followed by incubation with secondary antibodies and Hoechst for 2 h at RT. Slides were
458 mounted with Glycergel (Dako).

459 Organoids were fixed overnight at 4°C in 4% PFA for paraffin embedding and kept in
460 70% ethanol at 4°C before embedding. Samples were then embedded in paraffin,
461 sectioned (5 μm), mounted on glass slides, deparaffinized, and rehydrated. For
462 immunostaining, antigen retrieval was performed by incubating the sections for 10 min
463 in the microwave (850 W) in Sodium Citrate Buffer (10 mM Sodium Citrate, 0.05%
464 Tween 20, pH 6.0). After cooling, the sections were rinsed with PBS and blocked with
465 1% BSA and 10% horse serum PBS solution for 1 h at RT. Primary antibodies were
466 diluted (as described above) in the blocking solution and incubated overnight at 4°C. The
467 sections were rinsed three times in PBS and incubated with Hoechst and secondary
468 antibodies diluted in blocking solution for 1 h at room temperature. Slides were mounted
469 with Glycergel (Dako). Imaging was performed using a Zeiss LSM510 META confocal
470 microscope and a Leica DMI6000 microscope with DFC365FX camera. The antibodies
471 information is listed in the supplementary Table 1.

472

473 **Western blot**

474 Organoids were initially isolated (collagenase IV/dispase II solution, described above)
475 from at least 6 distinct wells and pooled together for protein extraction using RIPA buffer.
476 The protein concentration was determined according to Pierce 660 nm protein assay
477 reagent protocol (Thermo Scientific). Briefly, each sample's 30–50 μg of protein was
478 fractionated by 10% SDS–PAGE and blotted onto an Immobilon PVDF membrane
479 (Millipore). Blocking of non-specific binding sites were blocked by incubation with 5%
480 BSA in Tris-buffered saline (TBS) 0.1% Tween-20 for 1 h. Thereafter, the membrane
481 was incubated overnight at 4 °C with primary antibodies against p-ERK (1:1,000; Cell
482 Signaling; RRID:AB_2315112) and β-Actin (1:1,1000; Cell Signaling;
483 RRID:AB_2242334) in a blocking solution. Next, the membrane was incubated with
484 horseradish peroxidase-conjugated anti-rabbit (1:1,000; Cell Signaling;
485 RRID:AB_2099233) or anti-mouse antibody (1:1,000; Cell Signaling;
486 RRID:AB_330924) in a blocking solution, for 60 min at RT. The antigen-antibody
487 complexes were visualized using an enhanced chemiluminescence system (GE
488 Healthcare) and captured by Azure 500 system (Azure Biosystems).
489
490 **Iodide organification assay**
491 Thyroid organoids treated with cAMP, cAMP+4OHT, cAMP+4OHT+PD+LY and
492 cAMP+4OHT+PD+LY+VPA were tested for the ability of iodide uptake and
493 organification as previously described[37,57]. Briefly, cells were washed with HBSS and
494 incubated with 1 ml per well of an organification medium containing 1,000,000 c.p.m.
495 per ml ^{125}I (PerkinElmer) and 100 nM sodium iodide (NaI, Sigma) in HBSS for 2 h at 37
496 °C. After, the reaction was stopped by the addition of methimazole (MMI; 4 mM, Sigma).
497 After two cold PBS washes, cells were detached using trypsin/EDTA (Invitrogen). For
498 iodide uptake quantification, cells were collected, and radioactivity was measured using

499 a c-counter. Subsequently, proteins were precipitated by adding 1 mg of gamma-globulins
500 (Sigma) and 20% TCA followed by centrifugation at 2,000 r.p.m. for 10 min, at 4°C and
501 the radioactivity of protein-bound ^{125}I (PBI) was measured. Iodide organification was
502 calculated as an iodide uptake/PBI ratio and, the values were expressed as a percentage.
503 Cells were also treated with 1 mM sodium perchlorate (Nis inhibitor; NaClO4, Sigma-
504 Aldrich) and 2 mM MMI (Tpo inhibitor; Sigma-Aldrich) as iodide uptake and protein-
505 binding controls, respectively. The experiments were performed in triplicates for each
506 condition.
507

508 **Gene expression analysis**

509 Real-time PCR (RT-qPCR) was performed on cDNA from thyroid organoids from at least
510 three independent experiments. Total RNA was extracted from thyroid organoids by the
511 addition of lysis RLT Lysis buffer (Qiagen) + 1% 2-mercaptoethanol directly on the MTG
512 drop containing the organoids. RNA was isolated using the RNeasy micro kit (Qiagen)
513 according to the manufacturer's instructions. cDNA was generated by reverse
514 transcription using the Superscript II kit (Invitrogen). qPCR was performed on cDNA in
515 triplicates using Takyon™ No ROX SYBR 2X MasterMix blue dTTP (Eurogentec) and
516 CFX Connect Real-Time System (Biorad). Results are presented as linearized values
517 normalized to the housekeeping gene, β2-microglobulin and the indicated reference value
518 (2-DDCt). Primer sequences are described in supplementary Table 2.

519 **Bulk RNA sequencing and analysis**

520 Bulk RNA-seq was performed on day 31, using the cAMP, cAMP+4OHT (5 days) and
521 cAMP+4OHT+PD+LY (3 days) conditions (see protocol, Fig. 5A). RNA extraction was
522 performed as previously described (section "*Gene expression analysis"*), and
523 experiments were performed in duplicates. At least three distinct wells were pooled

524 together for each condition. RNA quality and concentration were evaluated using
525 Bioanalyser 2100 (Agilent) and RNA 6000 Nano Kit (Agilent). RNA integrity was
526 preserved, and no genomic DNA contamination was detected. Indexed cDNA libraries
527 were obtained using the TruSeq Stranded mRNA Sample Prep kit (Illumina) using an S2
528 flow cell, and sequences were produced using a 200 cycles reagent kit. The resulting high-
529 quality indexed cDNA libraries were quantified with the Quant-iT PicoGreen kit (Life
530 Sciences) and Infinite F200 Proplate reader (Tecan); DNA fragment size distribution was
531 examined with the 2100 Bioanalyzer (Agilent) using the DNA 1000 kit (Agilent).
532 Multiplexed libraries (10ρM) were loaded onto flow cells and sequenced on the HiSeq
533 1500 system (Illumina) in high-output mode using the HiSeq Cluster Kit v4 (Illumina).
534 The sequenced data were uploaded on the galaxy web platform version 22.05.1, and the
535 public server, Data independent acquisition proteomics workbench (RRID:SCR_021862,
536 https://usegalaxy.eu), was used for mapping and counting analysis. Approximately 10
537 million paired-end reads were obtained per sample. After the removal of low-quality
538 bases and Illumina adapter sequences using Trimmomatic software[97]
539 (RRID:SCR_011848), paired-end reads were mapped against the mouse reference
540 genome mm10 (GRCm38) using HISAT2 sofware[98] (RRID:SCR_015530), allowing soft
541 clipping. Raw read counts were obtained using HTseq (RRID:SCR_005514) count
542 software with unstranded option[99]. Low-expressed genes were filtered using the EdgeR
543 (RRID:SCR_012802) package in R Project for Statistical Computing
544 (RRID:SCR_001905; https://www.r-project.org). Then, differential expression analysis
545 was performed using DESeq2 package[100] (RRID:SCR_000154). Fold change and
546 adjusted p-value thresholds of 2 and 0.05, respectively were used to select differentially
547 expressed genes (DEG). Gene ontology and pathways enrichment analysis in up and
548 down differentially expressed gene lists was realized using EnrichR

549 (https://maayanlab.cloud/Enrichr/). Transformed counts corresponding to log2
550 (normalized counts +4) using the DESeq2 package were used for further analysis and
551 heatmap visualization. Thyroid differentiation score (TDS), Enhanced Thyroid
552 differentiation score (eTDS) and ERK activation score were calculated as previously
553 described[63]. The list of the genes used for the score's calculation is provided in
554 Supplementary Table 3.
555
556 **Data availability**
557 Bulk RNA-seq data have been deposited in the NCBI Gene Expression Omnibus (GEO;
558 RRID:SCR_005012) under accession number GSE228281.
559
560 **Statistical analysis**
561 All statistical analysis were performed using GraphPad Prism 9 (RRID:SCR_002798).
562 Comparison between two groups and its statistical significance was tested using the
563 unpaired *t*-test or nonparametric Mann-Whitney U test. In contrast, comparison between
564 multiple groups was performed using one-way ANOVA or nonparametric Kruskal-Wallis
565 test. Data are displayed as mean ± SD or median (IQR). Differences were considered
566 significant at $p<0.05$ and presented as follows: *$p < 0.05$, **$p < 0.01$, ***$p < 0.001$, ****p
567 < 0.0001. All the data presented are from at least three independent experiments.
568
569 **Acknowledgements and Funding**
570 The authors acknowledge the ULB flow cytometry platform (C. Dubois), the ULB
571 genomic core facility (F. Libert and A. Lefort), LiMIF platform for confocal microscopy
572 (J.-M. Vanderwinden). We acknowledge the funding agencies that supported this study.
573 The Belgian National Fund for Scientific Research (FNRS) (PDR T.0140.14; PDR

574 T.0230.18, CDR J.0068.22, Televie 7.4633.17/7.4526.19) and the Fonds
575 d'Encouragement à la Recherche de l'Université Libre de Bruxelles (FER-ULB). The
576 Belgian Fondation contre le cancer (F/2020/1402; V.D.). FNRS (Chargé de Recherche,
577 No.825745; M.R.). The cooperation program CAPES-WBI (S.C. and A.L.M). The
578 Brazilian National Council for Scientific and Technological Development (CNPq; M.R.
579 and A.L.M), the Coordination for the Improvement of Higher Education Personnel
580 (CAPES; M.R. and A.L.M), the Brazilian Society of Endocrinology and Metabolism
581 (SBEM; M.R. and A.L.M) and the Fundação de Amparo à Pesquisa do Estado do Rio
582 Grande do Sul (FAPERGS; A.L.M). S.C is Research Director at FNRS. M.R is researcher
583 at ULB.

584

585 **Author contributions**

586 H.L., S.C. and M.R. developed the project, designed the experiments and analyzed the
587 data. L.H., T.P., S.G. and J.H. generated the plasmids and the G4 Rosaluc mESC line.
588 M.R. and A.S. generated the G4 RosaLuc TRE-Nkx2-1-Pax8_bTg-NES-Braf^{V637E}-ERT^{2}
589 and TRE-Nkx2-1-Pax8_bTg-eGFP cell lines. H.L., M.R., B.F.F., A.S., O.M., L.C.,
590 M.K.P. B.A., L.C., performed the *in vitro* experiments and protocol set up. M.R. and P.G.
591 obtained confocal images. H.L., M.R. and A.T. performed bulk RNA-Sequencing and
592 analyzed the results. H.L. and A.T. performed the bioinformatics analysis. H.L. and M.R.
593 wrote the first draft and, A.L.M. and S.C. edited the manuscript. S.C., M.R. and A.L.M.
594 acquired funding for the project. All authors contributed to the article and approved the
595 submitted version.

596

597 **Competing interests**

598 All authors declare no competing interests.

599

600 **Correspondence** and requests for materials should be addressed to Mírian Romitti.

601

602 **REFERENCES**

603 1 Schutgens F, Clevers H. Human Organoids: Tools for Understanding Biology
604 and Treating Diseases. *Annual Review of Pathology: Mechanisms of Disease*
605 2020; **15**: 211–234.

606 2 Clevers H. Modeling Development and Disease with Organoids. *Cell* 2016; **165**:
607 1586–1597.

608 3 Kim J, Koo BK, Knoblich JA. Human organoids: model systems for human
609 biology and medicine. Nat Rev Mol Cell Biol. 2020; **21**: 571–584.

610 4 Boj SF, Hwang C-I, Baker LA, Chio IIC, Engle DD, Corbo V *et al.* Organoid
611 Models of Human and Mouse Ductal Pancreatic Cancer. *Cell* 2015; **160**: 324–
612 338.

613 5 Gao D, Vela I, Sboner A, Iaquinta PJ, Karthaus WR, Gopalan A *et al.* Organoid
614 Cultures Derived from Patients with Advanced Prostate Cancer. *Cell* 2014; **159**:
615 176–187.

616 6 Sato T, Stange DE, Ferrante M, Vries RGJ, van Es JH, van den Brink S *et al.*
617 Long-term Expansion of Epithelial Organoids From Human Colon, Adenoma,
618 Adenocarcinoma, and Barrett's Epithelium. *Gastroenterology* 2011; **141**: 1762–
619 1772.

620 7 van de Wetering M, Francies HE, Francis JM, Bounova G, Iorio F, Pronk A *et al.*
621 Prospective Derivation of a Living Organoid Biobank of Colorectal Cancer
622 Patients. *Cell* 2015; **161**: 933–945.

623 8 Drost J, Clevers H. Organoids in cancer research. *Nat Rev Cancer* 2018; **18**: 407–
624 418.
625 9 Gleave AM, Ci X, Lin D, Wang Y. A synopsis of prostate organoid
626 methodologies, applications, and limitations. *Prostate* 2020; **80**: 518–526.
627 10 Maenhoudt N, Vankelecom H. Protocol for establishing organoids from human
628 ovarian cancer biopsies. *STAR Protoc* 2021; **2**: 100429.
629 11 Gunti S, Hoke ATK, Vu KP, London NR. Organoid and Spheroid Tumor
630 Models: Techniques and Applications. *Cancers (Basel)* 2021; **13**: 874.
631 12 Saito Y, Onishi N, Takami H, Seishima R, Inoue H, Hirata Y *et al.* Development
632 of a functional thyroid model based on an organoid culture system. *Biochem*
633 *Biophys Res Commun* 2018; **497**: 783–789.
634 13 Chen D, Su X, Zhu L, Jia H, Han B, Chen H *et al.* Papillary thyroid cancer
635 organoids harboring BRAFV600E mutation reveal potentially beneficial effects
636 of BRAF inhibitor-based combination therapies. *J Transl Med* 2023; **21**: 9.
637 14 Vlachogiannis G, Hedayat S, Vatsiou A, Jamin Y, Fernández-Mateos J, Khan K
638 *et al.* Patient-derived organoids model treatment response of metastatic
639 gastrointestinal cancers. *Science (1979)* 2018; **359**: 920–926.
640 15 Drost J, van Jaarsveld RH, Ponsioen B, Zimberlin C, van Boxtel R, Buijs A *et al.*
641 Sequential cancer mutations in cultured human intestinal stem cells. *Nature*
642 2015; **521**: 43–47.
643 16 Matano M, Date S, Shimokawa M, Takano A, Fujii M, Ohta Y *et al.* Modeling
644 colorectal cancer using CRISPR-Cas9–mediated engineering of human intestinal
645 organoids. *Nat Med* 2015; **21**: 256–262.

646 17 Miura A, Yamada D, Nakamura M, Tomida S, Shimizu D, Jiang Y *et al.*
647 Oncogenic potential of human pluripotent stem cell-derived lung organoids with
648 <scp>HER2</scp> overexpression. *Int J Cancer* 2021; **149**: 1593–1604.
649 18 Nadauld LD, Garcia S, Natsoulis G, Bell JM, Miotke L, Hopmans ES *et al.*
650 Metastatic tumor evolution and organoid modeling implicate TGFBR2as a cancer
651 driver in diffuse gastric cancer. *Genome Biol* 2014; **15**: 428.
652 19 Li X, Nadauld L, Ootani A, Corney DC, Pai RK, Gevaert O *et al.* Oncogenic
653 transformation of diverse gastrointestinal tissues in primary organoid culture. *Nat*
654 *Med* 2014; **20**: 769–777.
655 20 Huang L, Holtzinger A, Jagan I, BeGora M, Lohse I, Ngai N *et al.* Ductal
656 pancreatic cancer modeling and drug screening using human pluripotent stem
657 cell– and patient-derived tumor organoids. *Nat Med* 2015; **21**: 1364–1371.
658 21 Lo Y-H, Karlsson K, Kuo CJ. Applications of organoids for cancer biology and
659 precision medicine. *Nat Cancer* 2020; **1**: 761–773.
660 22 Lim H, Devesa SS, Sosa JA, Check D, Kitahara CM. Trends in Thyroid Cancer
661 Incidence and Mortality in the United States, 1974-2013. *JAMA* 2017; **317**: 1338.
662 23 ROMITTI M, CEOLIN L, SIQUEIRA DR, FERREIRA CV, WAJNER SM,
663 MAIA AL. Signaling pathways in follicular cell-derived thyroid carcinomas. *Int*
664 *J Oncol* 2013; **42**: 19–28.
665 24 Kimura ET, Nikiforova MN, Zhu Z, Knauf JA, Nikiforov YE, Fagin JA. High
666 prevalence of BRAF mutations in thyroid cancer: genetic evidence for
667 constitutive activation of the RET/PTC-RAS-BRAF signaling pathway in
668 papillary thyroid carcinoma. *Cancer Res* 2003; **63**: 1454–7.
669 25 Fagin JA, Mitsiades N. Molecular pathology of thyroid cancer: diagnostic and
670 clinical implications. *Best Pract Res Clin Endocrinol Metab* 2008; **22**: 955–969.

671 26 Scheffel RS, Cristo AP de, Romitti M, Vargas CVF, Ceolin L, Zanella AB *et al.*
672 The BRAFV600E mutation analysis and risk stratification in papillary thyroid
673 carcinoma. *Arch Endocrinol Metab* 2020. doi:10.20945/2359-3997000000285.
674 27 Xing M. The T1799A BRAF mutation is not a germline mutation in familial
675 nonmedullary thyroid cancer. *Clin Endocrinol (Oxf)* 2005; **63**: 263–266.
676 28 Chakravarty D, Santos E, Ryder M, Knauf JA, Liao X-H, West BL *et al.* Small-
677 molecule MAPK inhibitors restore radioiodine incorporation in mouse thyroid
678 cancers with conditional BRAF activation. *Journal of Clinical Investigation*
679 2011; **121**: 4700–4711.
680 29 Zaman, Wu, Bivona. Targeting Oncogenic BRAF: Past, Present, and Future.
681 *Cancers (Basel)* 2019; **11**: 1197.
682 30 Agrawal N, Akbani R, Aksoy BA, Ally A, Arachchi H, Asa SL *et al.* Integrated
683 Genomic Characterization of Papillary Thyroid Carcinoma. *Cell* 2014; **159**: 676–
684 690.
685 31 Romei C, Fugazzola L, Puxeddu E, Frasca F, Viola D, Muzza M *et al.*
686 Modifications in the Papillary Thyroid Cancer Gene Profile Over the Last 15
687 Years. *J Clin Endocrinol Metab* 2012; **97**: E1758–E1765.
688 32 Sabra MM, Dominguez JM, Grewal RK, Larson SM, Ghossein RA, Tuttle RM *et*
689 *al.* Clinical Outcomes and Molecular Profile of Differentiated Thyroid Cancers
690 With Radioiodine-Avid Distant Metastases. *J Clin Endocrinol Metab* 2013; **98**:
691 E829–E836.
692 33 Xing M. BRAFV600E Mutation and Papillary Thyroid Cancer. *JAMA* 2013; **310**:
693 535.

694 34 Scheffel RS, Cristo AP de, Romitti M, Vargas CVF, Ceolin L, Zanella AB *et al.*
695 The BRAFV600E mutation analysis and risk stratification in papillary thyroid
696 carcinoma. *Arch Endocrinol Metab* 2021. doi:10.20945/2359-3997000000285.
697 35 Liu R, Bishop J, Zhu G, Zhang T, Ladenson PW, Xing M. Mortality Risk
698 Stratification by Combining *BRAF* V600E and *TERT* Promoter Mutations in
699 Papillary Thyroid Cancer. *JAMA Oncol* 2017; **3**: 202.
700 36 Boucai L, Seshan V, Williams M, Knauf JA, Saqcena M, Ghossein RA *et al.*
701 Characterization of Subtypes of BRAF-Mutant Papillary Thyroid Cancer Defined
702 by Their Thyroid Differentiation Score. *J Clin Endocrinol Metab* 2022; **107**:
703 1030–1039.
704 37 Antonica F, Kasprzyk DF, Opitz R, Iacovino M, Liao XH, Dumitrescu AM *et al.*
705 Generation of functional thyroid from embryonic stem cells. *Nature* 2012; **491**:
706 66–71.
707 38 Romitti M, Tourneur A, de Faria da Fonseca B, Doumont G, Gillotay P, Liao X-
708 H *et al.* Transplantable human thyroid organoids generated from embryonic stem
709 cells to rescue hypothyroidism. *Nat Commun* 2022; **13**: 7057.
710 39 Longmire TA, Ikonomou L, Hawkins F, Christodoulou C, Cao Y, Jean JC *et al.*
711 Efficient derivation of purified lung and thyroid progenitors from embryonic
712 stem cells. *Cell Stem Cell* 2012; **10**: 398–411.
713 40 Ma R, Latif R, Davies TF. Human embryonic stem cells form functional thyroid
714 follicles. *Thyroid* 2015; **25**: 455–461.
715 41 Ma R, Latif R, Davies TF. Thyroid follicle formation and thyroglobulin
716 expression in multipotent endodermal stem cells. *Thyroid* 2013; **23**: 385–391.

717 42 Ma R, Morshed SA, Latif R, Davies TF. TAZ Induction Directs Differentiation
718 of Thyroid Follicular Cells from Human Embryonic Stem Cells. *Thyroid* 2017;
719 **27**: 292–299.
720 43 Ma R, Shi R, Morshed SA, Latif R, Davies TF. Derivation and 97% Purification
721 of Human Thyroid Cells From Dermal Fibroblasts. *Front Endocrinol (Lausanne)*
722 2020; **11**: 446.
723 44 Kurmann AA, Serra M, Hawkins F, Rankin SA, Mori M, Astapova I *et al.*
724 Regeneration of Thyroid Function by Transplantation of Differentiated
725 Pluripotent Stem Cells. *Cell Stem Cell* 2015; **17**: 527–542.
726 45 Serra M, Alysandratos KD, Hawkins F, McCauley KB, Jacob A, Choi J *et al.*
727 Pluripotent stem cell differentiation reveals distinct developmental pathways
728 regulating Lung-Versus Thyroid-Lineage specification. *Development*
729 *(Cambridge)* 2017; **144**: 3879–3893.
730 46 Dame K, Cincotta S, Lang AH, Sanghrajka RM, Zhang L, Choi J *et al.* Thyroid
731 Progenitors Are Robustly Derived from Embryonic Stem Cells through
732 Transient, Developmental Stage-Specific Overexpression of Nkx2-1. *Stem Cell*
733 *Reports* 2017; **8**: 216–225.
734 47 Ogundipe VML, Groen AH, Hosper N, Nagle PWK, Hess J, Faber H *et al.*
735 Generation and Differentiation of Adult Tissue-Derived Human Thyroid
736 Organoids. *Stem Cell Reports* 2021; **16**: 913–925.
737 48 Liang J, Qian J, Yang L, Chen X, Wang X, Lin X *et al.* Modeling Human
738 Thyroid Development by Fetal Tissue-Derived Organoid Culture. *Advanced*
739 *Science* 2022; **9**. doi:10.1002/advs.202105568.
740 49 van der Vaart J, Bosmans L, Sijbesma SF, Knoops K, van de Wetering WJ, Otten
741 HG *et al.* Adult mouse and human organoids derived from thyroid follicular cells

742 and modeling of Graves' hyperthyroidism. *Proceedings of the National Academy*
743 *of Sciences* 2021; **118**. doi:10.1073/pnas.2117017118.
744 50 Chen D, Tan Y, Li Z, Li W, Yu L, Chen W *et al.* Organoid Cultures Derived
745 From Patients With Papillary Thyroid Cancer. *J Clin Endocrinol Metab* 2021;
746 **106**: 1410–1426.
747 51 Sondorp LHJ, Ogundipe VML, Groen AH, Kelder W, Kemper A, Links TP *et al.*
748 Patient-Derived Papillary Thyroid Cancer Organoids for Radioactive Iodine
749 Refractory Screening. *Cancers (Basel)* 2020; **12**: 3212.
750 52 Pecce V, Sponziello M, Bini S, Grani G, Durante C, Verrienti A. Establishment
751 and maintenance of thyroid organoids from human cancer cells. *STAR Protoc*
752 2022; **3**: 101393.
753 53 Chen D, Su X, Zhu L, Jia H, Han B, Chen H *et al.* Papillary thyroid cancer
754 organoids harboring BRAFV600E mutation reveal potentially beneficial effects
755 of BRAF inhibitor-based combination therapies. *J Transl Med* 2023; **21**: 9.
756 54 Yang H, Liang Q, Zhang J, Liu J, Wei H, Chen H *et al.* Establishment of
757 papillary thyroid cancer organoid lines from clinical specimens. *Front*
758 *Endocrinol (Lausanne)* 2023; **14**. doi:10.3389/fendo.2023.1140888.
759 55 Veschi V, Turdo A, Modica C, Verona F, Di Franco S, Gaggianesi M *et al.*
760 Recapitulating thyroid cancer histotypes through engineering embryonic stem
761 cells. *Nat Commun* 2023; **14**: 1351.
762 56 Antonica F, Kasprzyk DF, Schiavo AA, Romitti M, Costagliola S. Generation of
763 Functional Thyroid Tissue Using 3D-Based Culture of Embryonic Stem Cells.
764 2017, pp 85–95.
765 57 Romitti M, Eski SE, Fonseca BF, Gillotay P, Singh SP, Costagliola S. Single-
766 Cell Trajectory Inference Guided Enhancement of Thyroid Maturation In Vitro

767 Using TGF-Beta Inhibition. *Front Endocrinol (Lausanne)* 2021; **12**.
768 doi:10.3389/fendo.2021.657195.
769 58 Ortiz O, Wurst W, Kühn R. Reversible and tissue-specific activation of MAP
770 kinase signaling by tamoxifen in braf ^{V637} ER ^{T2} mice. *genesis* 2013; **51**: 448–
771 455.
772 59 Knauf JA, Ma X, Smith EP, Zhang L, Mitsutake N, Liao X-H *et al.* Targeted
773 Expression of BRAFV600E in Thyroid Cells of Transgenic Mice Results in
774 Papillary Thyroid Cancers that Undergo Dedifferentiation. *Cancer Res* 2005; **65**:
775 4238–4245.
776 60 Tang W-W, Huang C, Tang C, Xu J, Wang H. Galectin-3 may serve as a
777 potential marker for diagnosis and prognosis in papillary thyroid carcinoma: a
778 meta-analysis. *Onco Targets Ther* 2016; : 455.
779 61 Xia S, Wang C, Postma EL, Yang Y, Ni X, Zhan W. Fibronectin 1 promotes
780 migration and invasion of papillary thyroid cancer and predicts papillary thyroid
781 cancer lymph node metastasis. *Onco Targets Ther* 2017; **Volume 10**: 1743–1755.
782 62 Sponziello M, Rosignolo F, Celano M, Maggisano V, Pecce V, De Rose RF *et al.*
783 Fibronectin-1 expression is increased in aggressive thyroid cancer and favors the
784 migration and invasion of cancer cells. *Mol Cell Endocrinol* 2016; **431**: 123–132.
785 63 Dunn LA, Sherman EJ, Baxi SS, Tchekmedyian V, Grewal RK, Larson SM *et al.*
786 Vemurafenib Redifferentiation of *BRAF* Mutant, RAI-Refractory Thyroid
787 Cancers. *J Clin Endocrinol Metab* 2019; **104**: 1417–1428.
788 64 Kogai T, Brent GA. The sodium iodide symporter (NIS): Regulation and
789 approaches to targeting for cancer therapeutics. *Pharmacol Ther* 2012; **135**: 355–
790 370.

791 65 Azouzi N, Cailloux J, Cazarin JM, Knauf JA, Cracchiolo J, Al Ghuzlan A *et al.*
792 NADPH Oxidase NOX4 Is a Critical Mediator of BRAF ^{V600E} -Induced
793 Downregulation of the Sodium/Iodide Symporter in Papillary Thyroid
794 Carcinomas. *Antioxid Redox Signal* 2017; **26**: 864–877.
795 66 Saqcena M, Leandro-Garcia LJ, Maag JLV, Tchekmedyian V, Krishnamoorthy
796 GP, Tamarapu PP *et al.* SWI/SNF Complex Mutations Promote Thyroid Tumor
797 Progression and Insensitivity to Redifferentiation Therapies. *Cancer Discov*
798 2021; **11**: 1158–1175.
799 67 Qiu W, Yang Z, Fan Y, Zheng Q. ZNRF3 is downregulated in papillary thyroid
800 carcinoma and suppresses the proliferation and invasion of papillary thyroid
801 cancer cells. *Tumor Biology* 2016; **37**: 12665–12672.
802 68 Han J, Chen M, Wang Y, Gong B, Zhuang T, Liang L *et al.* Identification of
803 Biomarkers Based on Differentially Expressed Genes in Papillary Thyroid
804 Carcinoma. *Sci Rep* 2018; **8**: 9912.
805 69 Yoo S-K, Song YS, Lee EK, Hwang J, Kim HH, Jung G *et al.* Integrative
806 analysis of genomic and transcriptomic characteristics associated with
807 progression of aggressive thyroid cancer. *Nat Commun* 2019; **10**: 2764.
808 70 Davies H, Bignell GR, Cox C, Stephens P, Edkins S, Clegg S *et al.* Mutations of
809 the BRAF gene in human cancer. *Nature* 2002; **417**: 949–954.
810 71 Dhomen N, Marais R. New insight into BRAF mutations in cancer. *Curr Opin*
811 *Genet Dev* 2007; **17**: 31–39.
812 72 Nikiforov YE, Nikiforova MN. Molecular genetics and diagnosis of thyroid
813 cancer. *Nat Rev Endocrinol* 2011; **7**: 569–580.

814 73 Cheng L, Lopez-Beltran A, Massari F, MacLennan GT, Montironi R. Molecular
815 testing for BRAF mutations to inform melanoma treatment decisions: a move
816 toward precision medicine. *Modern Pathology* 2018; **31**: 24–38.
817 74 Schirripa M, Biason P, Lonardi S, Pella N, Pino MS, Urbano F *et al.* Class 1, 2,
818 and 3 BRAF-Mutated Metastatic Colorectal Cancer: A Detailed Clinical,
819 Pathologic, and Molecular Characterization. *Clinical Cancer Research* 2019; **25**:
820 3954–3961.
821 75 Pisapia P, Pepe F, Malapelle U, Troncone G. Mutations in Lung Cancer. *Acta*
822 *Cytol* 2019; **63**: 247–250.
823 76 Pisapia P, Pepe F, Iaccarino A, Sgariglia R, Nacchio M, Russo G *et al.* BRAF: A
824 Two-Faced Janus. *Cells* 2020; **9**: 2549.
825 77 Pavlick AC, Fecher L, Ascierto PA, Sullivan RJ. Frontline Therapy for BRAF-
826 Mutated Metastatic Melanoma: How Do You Choose, and Is There One Correct
827 Answer? *American Society of Clinical Oncology Educational Book* 2019; : 564–
828 571.
829 78 Anguera G, Majem M. BRAF inhibitors in metastatic non-small cell lung cancer.
830 *J Thorac Dis* 2018; **10**: 589–592.
831 79 Haugen BR, Alexander EK, Bible KC, Doherty GM, Mandel SJ, Nikiforov YE *et*
832 *al.* 2015 American Thyroid Association Management Guidelines for Adult
833 Patients with Thyroid Nodules and Differentiated Thyroid Cancer: The American
834 Thyroid Association Guidelines Task Force on Thyroid Nodules and
835 Differentiated Thyroid Cancer. *Thyroid* 2016; **26**: 1–133.
836 80 Schmidbauer B, Menhart K, Hellwig D, Grosse J. Differentiated Thyroid
837 Cancer—Treatment: State of the Art. *Int J Mol Sci* 2017; **18**: 1292.

838 81 Kim TY, Kim WG, Kim WB, Shong YK. Current Status and Future Perspectives
839 in Differentiated Thyroid Cancer. *Endocrinology and Metabolism* 2014; **29**: 217.
840 82 Ahn B-C. Personalized Medicine Based on Theranostic Radioiodine Molecular
841 Imaging for Differentiated Thyroid Cancer. *Biomed Res Int* 2016; **2016**: 1–9.
842 83 Paeng JC, Kang KW, Park DJ, Oh SW, Chung J-K. Alternative Medical
843 Treatment for Radioiodine-Refractory Thyroid Cancers. *Nucl Med Mol Imaging*
844 2011; **45**: 241–247.
845 84 Brose MS, Nutting CM, Jarzab B, Elisei R, Siena S, Bastholt L *et al.* Sorafenib in
846 radioactive iodine-refractory, locally advanced or metastatic differentiated
847 thyroid cancer: a randomised, double-blind, phase 3 trial. *The Lancet* 2014; **384**:
848 319–328.
849 85 Schlumberger M, Tahara M, Wirth LJ, Robinson B, Brose MS, Elisei R *et al.*
850 Lenvatinib versus Placebo in Radioiodine-Refractory Thyroid Cancer. *New*
851 *England Journal of Medicine* 2015; **372**: 621–630.
852 86 Ho AL, Grewal RK, Leboeuf R, Sherman EJ, Pfister DG, Deandreis D *et al.*
853 Selumetinib-Enhanced Radioiodine Uptake in Advanced Thyroid Cancer. *New*
854 *England Journal of Medicine* 2013; **368**: 623–632.
855 87 Rothenberg SM, Daniels GH, Wirth LJ. Redifferentiation of Iodine-Refractory
856 BRAF V600E-Mutant Metastatic Papillary Thyroid Cancer with Dabrafenib—
857 Response. *Clinical Cancer Research* 2015; **21**: 5640–5641.
858 88 Buffet C, Wassermann J, Hecht F, Leenhardt L, Dupuy C, Groussin L *et al.*
859 Redifferentiation of radioiodine-refractory thyroid cancers. *Endocr Relat Cancer*
860 2020; **27**: R113–R132.

861 89 Riesco-Eizaguirre G, Santisteban P. A perspective view of sodium iodide
862 symporter research and its clinical implications. *Eur J Endocrinol* 2006; **155**:
863 495–512.
864 90 Czarnecka AM, Bartnik E, Fiedorowicz M, Rutkowski P. Targeted Therapy in
865 Melanoma and Mechanisms of Resistance. *Int J Mol Sci* 2020; **21**: 4576.
866 91 Flaherty KT, Infante JR, Daud A, Gonzalez R, Kefford RF, Sosman J *et al.*
867 Combined BRAF and MEK Inhibition in Melanoma with BRAF V600
868 Mutations. *New England Journal of Medicine* 2012; **367**: 1694–1703.
869 92 Larkin J, Ascierto PA, Dréno B, Atkinson V, Liszkay G, Maio M *et al.*
870 Combined Vemurafenib and Cobimetinib in BRAF-Mutated Melanoma. *New*
871 *England Journal of Medicine* 2014; **371**: 1867–1876.
872 93 Dummer R, Ascierto PA, Gogas HJ, Arance A, Mandala M, Liszkay G *et al.*
873 Encorafenib plus binimetinib versus vemurafenib or encorafenib in patients with
874 BRAF -mutant melanoma (COLUMBUS): a multicentre, open-label, randomised
875 phase 3 trial. *Lancet Oncol* 2018; **19**: 603–615.
876 94 Smalley KSM. Increased immunity and BRAF inhibition: Yet another argument
877 for combination therapy? *Pharmacol Res* 2016; **113**: 719–720.
878 95 Roskoski R. Targeting oncogenic Raf protein-serine/threonine kinases in human
879 cancers. *Pharmacol Res* 2018; **135**: 239–258.
880 96 Haenebalcke L, Goossens S, Naessens M, Kruse N, Ghahremani MF, Bartunkova
881 S *et al.* Efficient ROSA26-Based Conditional and/or Inducible Transgenesis
882 Using RMCE-Compatible F1 Hybrid Mouse Embryonic Stem Cells. *Stem Cell*
883 *Rev Rep* 2013; **9**: 774–785.
884 97 Bolger AM, Lohse M, Usadel B. Trimmomatic: a flexible trimmer for Illumina
885 sequence data. *Bioinformatics* 2014; **30**. doi:10.1093/bioinformatics/btu170.

98 Kim D, Langmead B, Salzberg SL. HISAT: a fast spliced aligner with low memory requirements. *Nat Methods* 2015; **12**. doi:10.1038/nmeth.3317.

99 Hao Y, Hao S, Andersen-Nissen E, Mauck WM, Zheng S, Butler A *et al.* Integrated analysis of multimodal single-cell data. *Cell* 2021; **184**: 3573-3587.e29.

100 Love MI, Huber W, Anders S. Moderated estimation of fold change and dispersion for RNA-seq data with DESeq2. *Genome Biol* 2014; **15**: 550.

911 **FIGURES**

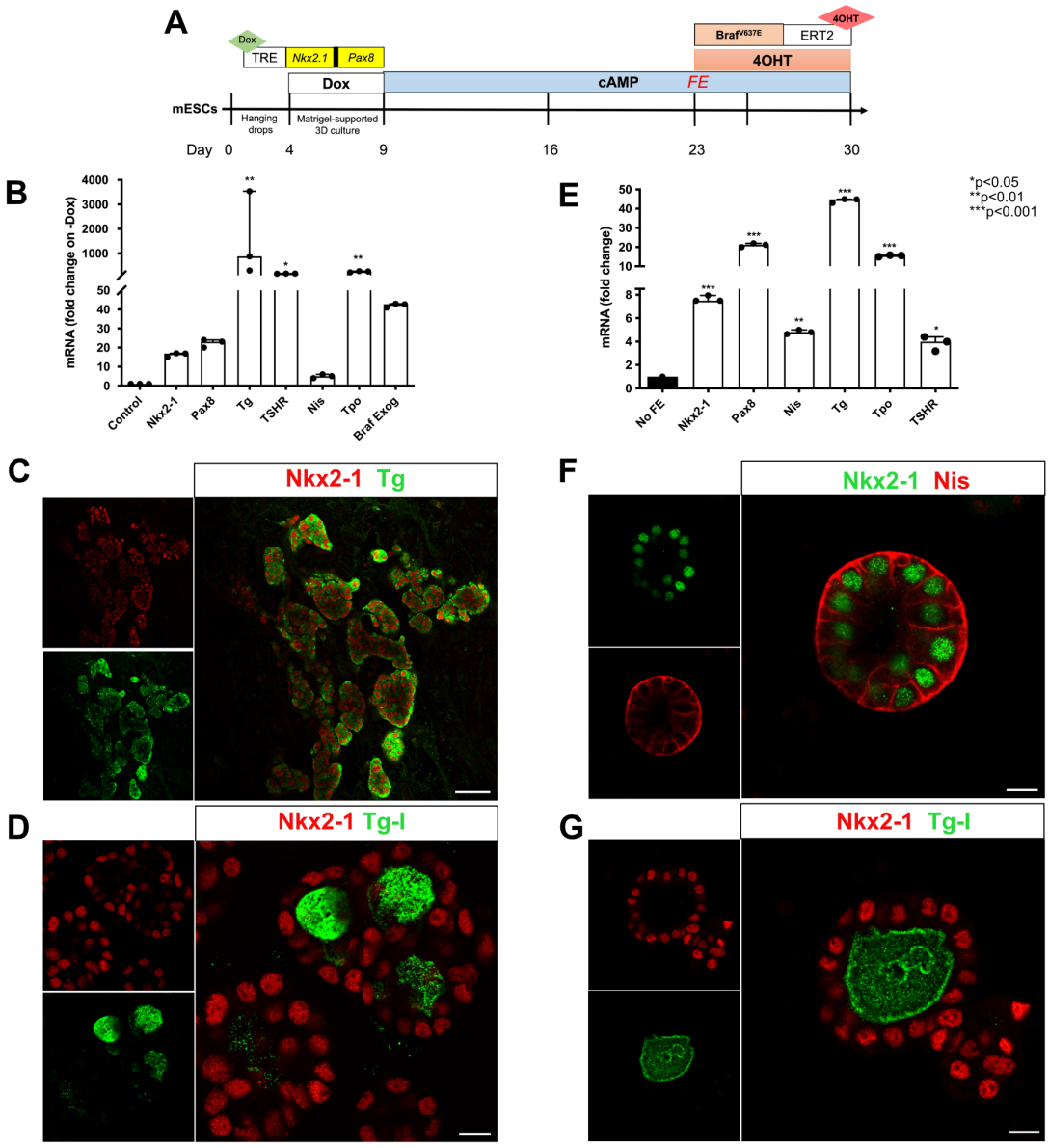

912

913 **Fig. 1 mESC_Nkx2-1/Pax8_bTg_Braf^{V637E} cell line differentiation into thyroid**
914 **organoids.** Scheme of the thyroid differentiation protocol and Braf^{V637E} induction in
915 mature thyroid follicles (A). Differentiation of mESC_Nkx2-1/Pax8_bTg_Braf^{V637E} cell
916 line promotes expression of the main thyroid genes and Braf exogenous (B).
917 Immunofluorescence staining showing Nkx2-1 and Tg co-expressing cells organized in
918 follicular structures (C), which are accumulating the thyroid hormone precursor, Tg-I,
919 inside the lumen compartment (D). The follicular enrichment (FE) procedure
920 significantly increased the expression levels of thyroid genes (E) while keeping the

921 structural organization of the follicles (F) and its functionality evidenced by Tg-I
922 accumulation (G). Scale bars, 50 µm and 10 µm for high magnification follicles.
923

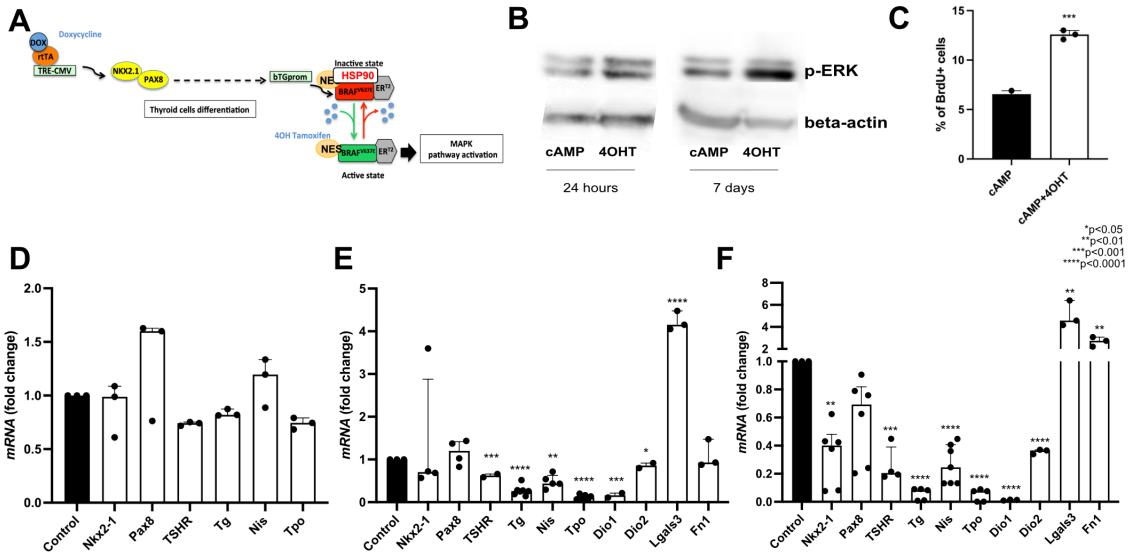

924

925 **Fig. 2 Effect of the Braf^{V637E} oncogene induction on mature thyroid follicles.**
926 Schematic representation of thyroid differentiation, Braf^{V637E} oncogene expression and
927 its activation under specific treatment conditions (A). Western blot demonstrates an
928 increase of p-ERK protein at 24 hours and 7 days after the addition of 4OHT (Tamoxifen)
929 to the organoids culture (B). Percentage of BrDU+ cells between control (cAMP) and
930 Braf-induced (4OHT; 6 days) condition (C). mRNA expression analysis showing the
931 inhibitory effect of Braf^{V637E}-oncogene induction on thyroid genes after 6 hours (D), 48
932 hours (E) and 7 days (F).

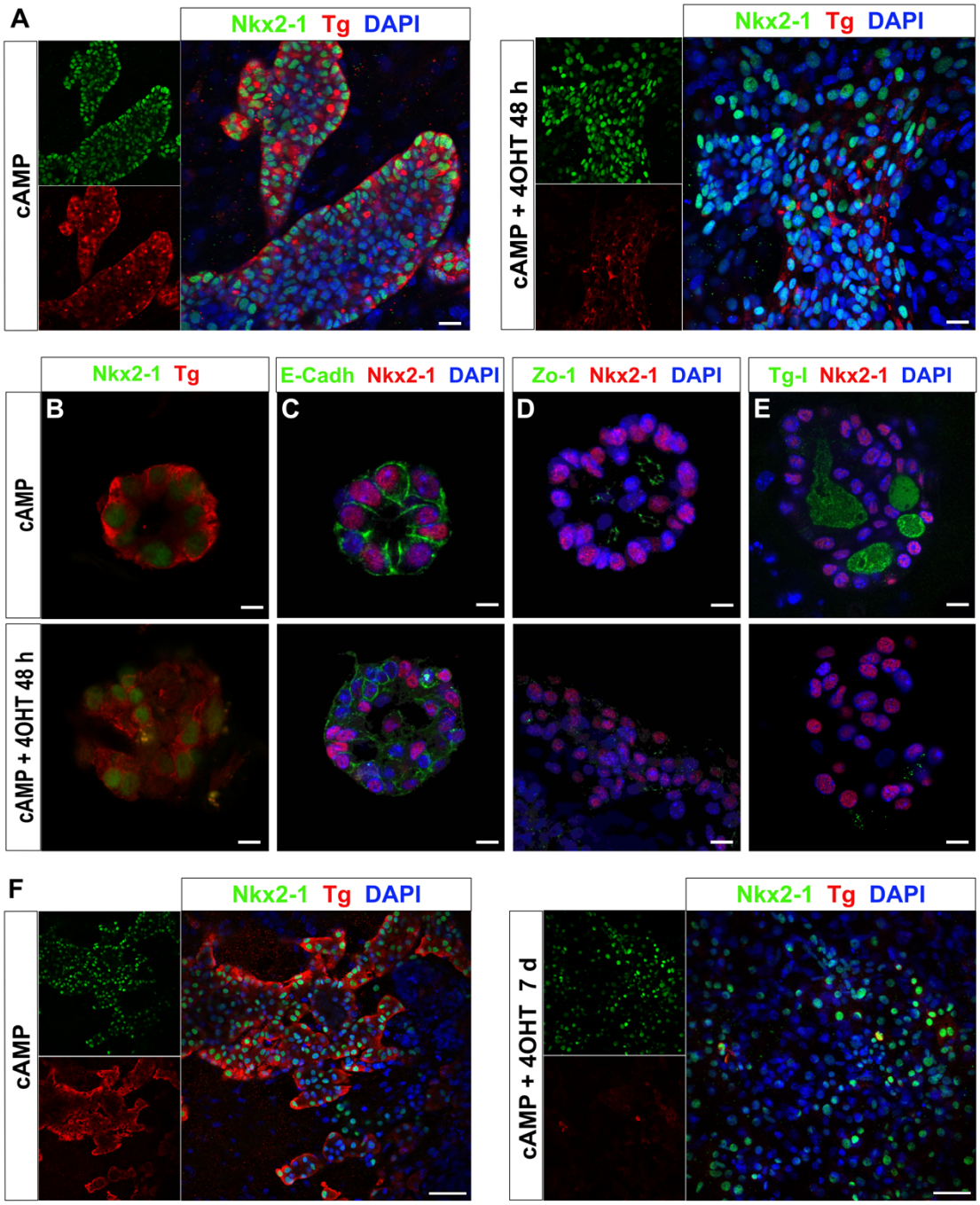

933

934 **Fig. 3 Morphological changes caused by Braf^{V637E} activation on thyroid follicles.**
935 Control thyroid cells show follicular organization with Nkx2-1 nuclear expression and
936 Tg accumulation in the luminal compartment. In contrast, after 48 h of Braf oncogene
937 induction by 4OHT, most of the cells are not organized into follicular structures and a
938 great proportion of cells is expressing very low levels of Tg (A). Higher magnification
939 images showing the follicular organization of the thyroid cells in the control condition

940 (48 h), with proper expression of Nk2x-1 and/or Tg (B), E-cadherin (C), Zo-1 (D) and
941 Tg-I (E) accumulation in the lumen. While in the 4OHT condition the follicular
942 organization is disrupted as well as its function. Nkx2-1 and Tg staining in control and
943 Braf-induced cells for 7 days shows clear changes in thyroid morphology evidenced by
944 the heterogeneity of Nkx2-1 cells which mostly do not express Tg or at low levels, while
945 some groups cells continue to co-express Tg (F). Scale bars, 20 µm (A), 10 µm (B-E) and
946 50 µm (F).
947

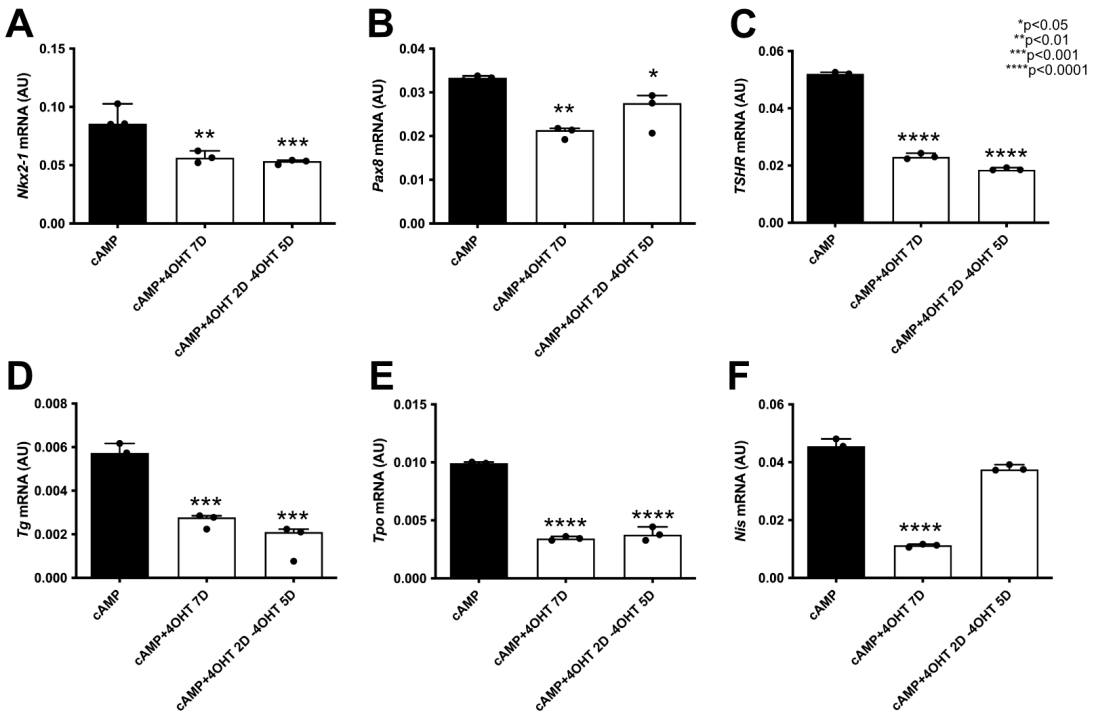

948

949 **Fig. 4 4OHT interruption does not restore the thyroid gene expression levels.** The
950 induction of Braf^{V637E} for 2 days followed by removal of 4OHT for 5 days shows that it
951 is not enough to recover the levels of *Nkx2-1* (A), *Pax8* (B), *TSHR* (C), *Tg* (D), *Tpo* (E)
952 genes to the control levels. However, it led to an increase of *Nis* expression (F) close to
953 control values.

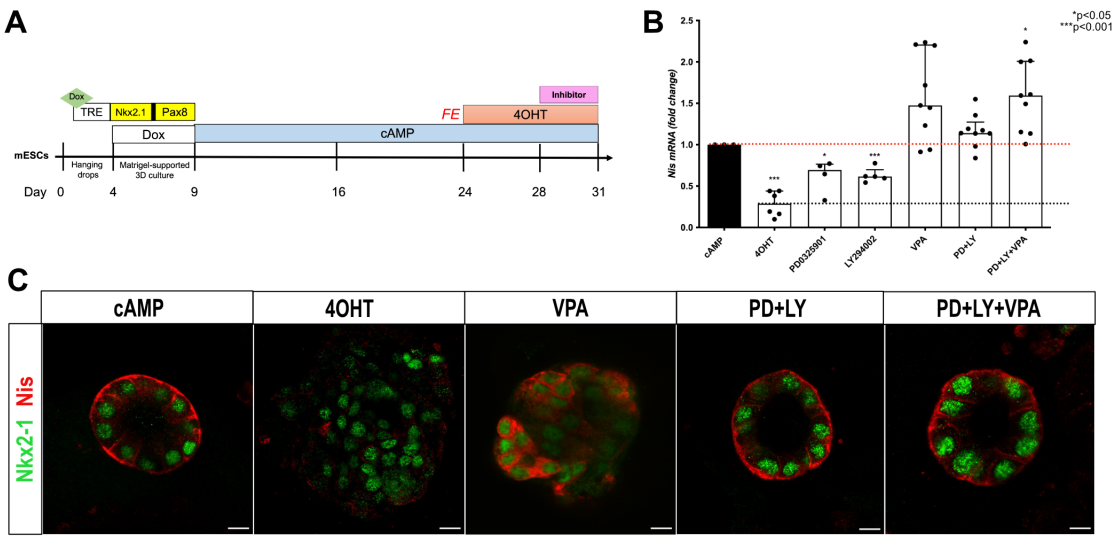

954

955 **Fig. 5 Drug screening reveals that VPA and MAPK/PI3K inhibition can restore Nis**
956 **expression in Braf-induced cells.** Schematic representation of the protocol used for drug
957 screening experiments (A). qPCR data show that inhibition of MAPK (PD0325901) and
958 PI3K (LY294002) pathways isolated increase but do not restore *Nis* expression to control
959 levels. However, when combined, the levels are like the controls. On the other hand, the
960 HDAC inhibitor (VPA) can recover Nis expression (B) by itself. Nkx2-1 and Nis
961 immunostaining shows the downregulation of the transporter in 4OHT condition, which
962 is restored by VPA treatment. However, the expression pattern differs from the control
963 conditions. Co-inhibition of MAPK and PI3K pathways associated or not to VPA
964 treatment restores of Nis protein expression while follicular structures are observed (C).
965 Scale bars, 10 µm.

966

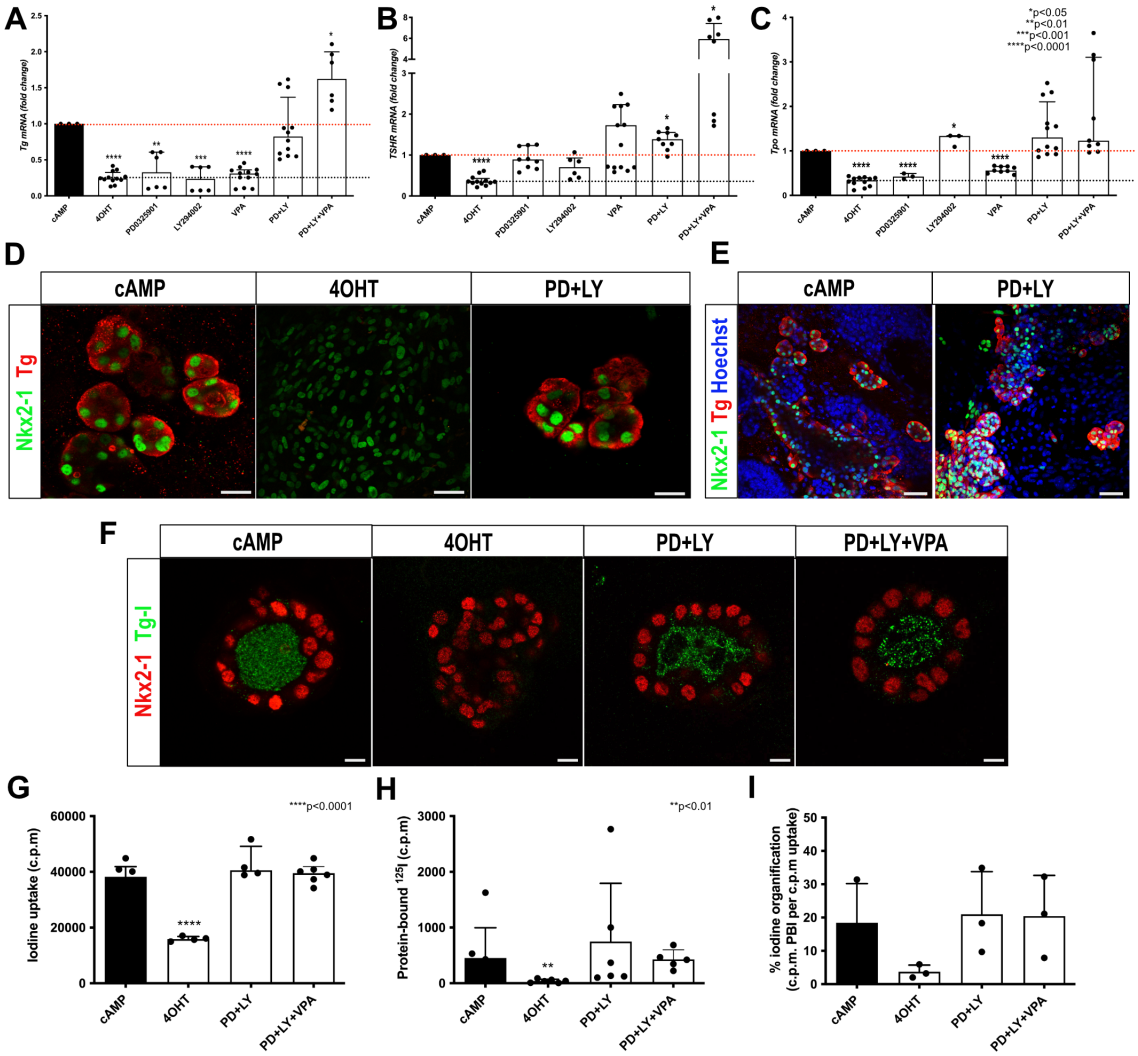

Fig. 6 MAPK and PI3K inhibition cause thyroid redifferentiation and function recovery of Braf-expressing cells. mRNA expression analysis shows that PD0325901 and LY294002 co-treatment recover the *Tg* (A), *TSHR* (B), and *Tpo* (C) gene expression to control levels. Immunostaining for Nkx2-1 and Tg shows that protein levels are similar to control and that follicular organization is restored under such treatment conditions (D, E). Tg-I accumulation in the lumen of the restored follicles is observed under PD+LY and PD+LY+VPA conditions (F). Organification assay shows a recovery of Iodine uptake (G), Protein-bound to 125I (H), and % of iodine Organification (I) in the inhibitor's conditions. Scale bars, 50 µm (E), 20 µm (D) and 10 µm for high magnification follicles (F).

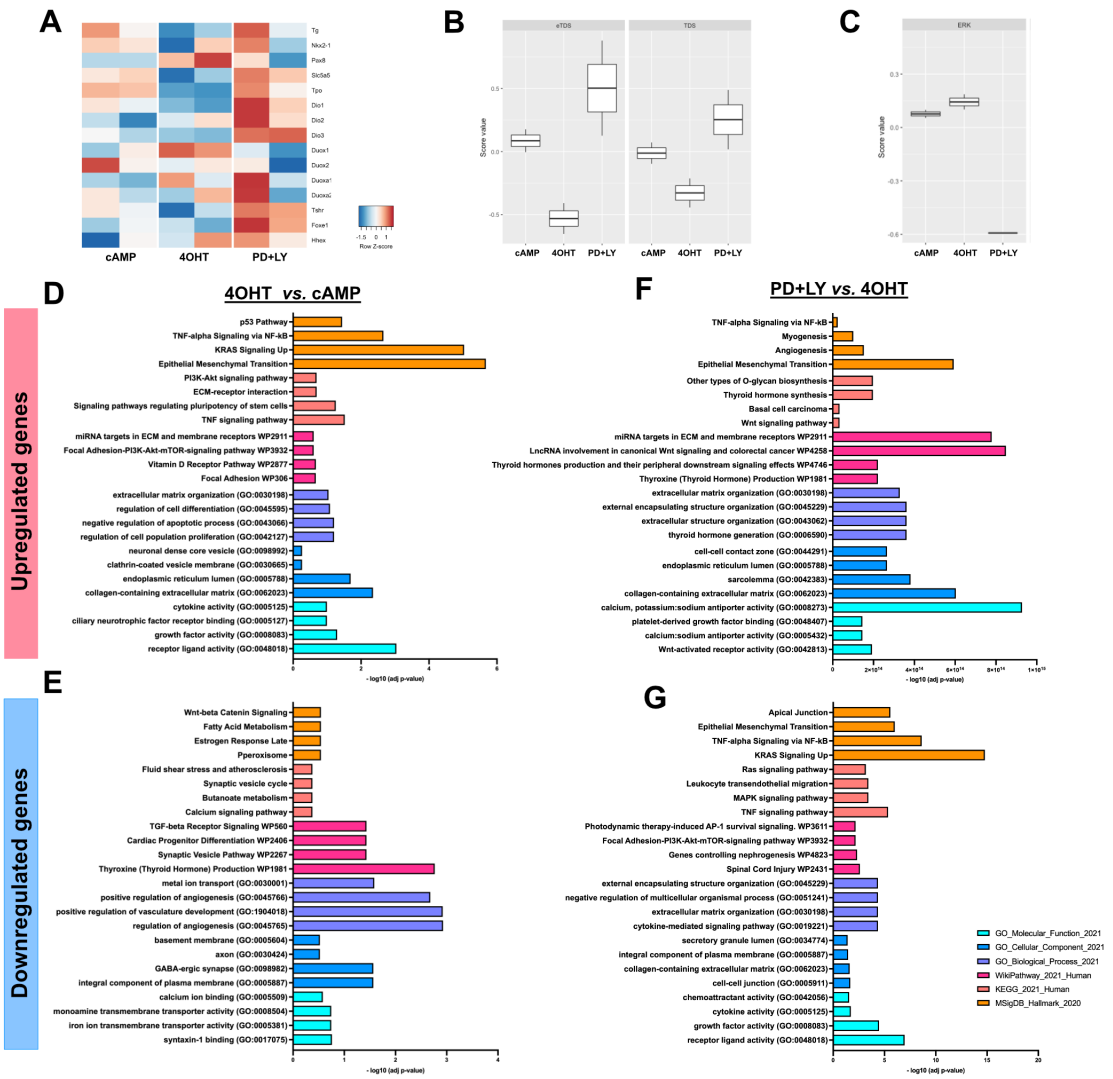

Fig. 7 Transcriptomics analysis confirms thyroid redifferentiation of Braf^{V637E}-expressing cells treated with MAPK and PI3K inhibitors and suggests by which mechanisms. Heatmap of normalized bulk RNA-Seq expression of normal thyroid cells (cAMP), Braf^{V637E} expressing cells (4OHT), and Braf^{V637E} expressing cells treated with PD0325901+LY204002 inhibitors. Rows represent markers and columns represent specific conditions. Color values in the heatmap represent mean expression levels (A). Thyroid differentiation (eTDS and TDS) (B) and ERK (C) scores were calculated among the different conditions. Classification of upregulated and downregulated genes comparing 4OHT *vs.* cAMP (D, E) and PD+LY *vs.* 4OHT (F, G). Colors represent the classification method and scale the -log10 (adj p-value).